Journal Pre-proofs

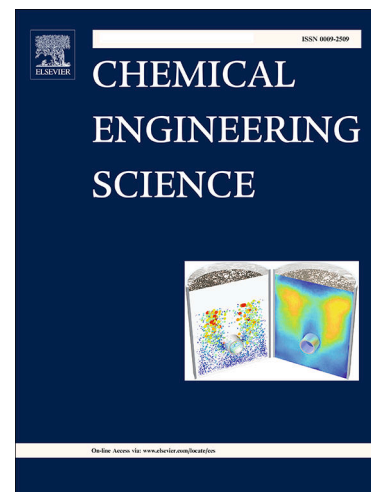CO$_2$ Capture with Room Temperature Ionic Liquids; Coupled Absorption/ Desorption and Single Module Absorption in Membrane Contactor

Sohaib Qazi, Jose Manuel Vadillo, Lucía Gómez-Coma, Jonathan Albo, Stéphanie Druon-Bocquet, Angel Irabien, José Sanchez-Marcano

Please cite this article as: S. Qazi, J. Manuel Vadillo, L. Gómez-Coma, J. Albo, S. Druon-Bocquet, A. Irabien, J. Sanchez-Marcano, CO$_2$ Capture with Room Temperature Ionic Liquids; Coupled Absorption/Desorption and Single Module Absorption in Membrane Contactor, *Chemical Engineering Science* (2020), doi: https://doi.org/ 10.1016/j.ces.2020.115719

CO$_2$ Capture with Room Temperature Ionic Liquids; Coupled Absorption/Desorption and Single Module Absorption in Membrane Contactor

Sohaib Qazi[1], Jose Manuel Vadillo[2], Lucía Gómez-Coma[2], Jonathan Albo[2], Stéphanie Druon-Bocquet[1], Angel Irabien[2], José Sanchez-Marcano[1]

1 : Institut Européen des Membranes, IEM – UMR 5635, CNRS, ENSCM, Université de Montpellier, Montpellier, France.

2 : Chemical and Biomolecular Engineering Department, Universidad de Cantabria, Av. Los Castros, 39005 Santander, Spain.

Abstract

A membrane gas CO$_2$ capture setup, based on the concept of single module absorption and single cycle coupled absorption/desorption, was developed in this work. Ionic liquids (ILs) 1-ethyl-3-methylimidazolium methylsulfate ([emim][MS]) and 1-ethyl-3-methylimidazolium dicyanamide ([emim][DCA]) were used as absorbents. The CO$_2$ absorption rate decreased initially and reached to a nearly constant value achieving pseudo steady state. Coupled absorption/desorption revealed very high performance by retaining 82% and 66% absorption efficiency, for [emim][MS] and [emim][DCA], respectively, even after 70 minutes of operation. Mass transfer coefficients of the coupled absorption/desorption at pseudo steady state were 9 and 5 folds higher than single module absorption, for [emim][MS] and [emim][DCA], respectively. Parametric analysis for the membrane absorber outlet concentration and optimization of the parameters to achieve zero concentration at the membrane stripper outlet were studied in simulations. As a conclusion, coupled absorption/desorption in combination with ILs, can be considered very suitable for continuous post-combustion carbon capture.

Key words: Coupled Absorption/Desorption, Pseudo Steady State Modelling, Carbon Capture, Membrane Contactors, Imidazolium Ionic Liquids

Nomenclature

A	Area (m^2)		A	Membrane absorber
C	Concentration ($mol\,m^{-3}$)		CO_2	Carbon dioxide
d	Diameter (m)		exp	Experimental
D	Diffusivity ($cm^2\,s^{-1}$)		g	Gas
E	Enhancement factor (-)		h	Hydraulic
H_d	Dimensionless Henry's law constant (-)		i	Inner
j	Molar Flux ($mol\,m^{-2}\,s^{-1}$)		in	Inlet
K	Mass transfer coefficient ($m\,s^{-1}$)		IL	Ionic Liquid
k	Local mass transfer coefficient ($m\,s^{-1}$)		l	Liquid
L	Length of membrane(m)		lm	Log mean
M	Molar weight ($kg\,mol^{-1}$)		m	membrane
N	Number of fibers (-)		out	Outlet
ñ	Number of moles (mol)		o	Outer
P	Pressure (Pa)		ov	Overall
Q	Volumetric flowrate ($m^3\,s^{-1}$)		r	Radial coordinate
Ŕ	Perfect gas constant ($m^3\,Pa\,mol^{-1}.K^{-1}$)		ř	Reservoir
r	Radius (m)		S	Membrane stripper
R_e	Reynolds number (-)		z	Axial coordinate
S_c	Schmidt number (-)			

Greek symbols

S_h	Sherwood number (-)		α	CO_2 loading ($mol\,mol^{-1}$)
t	Time(s)		ρ	Density ($g\,cm^{-3}$)
T	Temperature (K)		ε	Membrane porosity (-)
U	Interstitial velocity ($m\,s^{-1}$)		τ	Membrane tortuosity (-)
v	Molar volume ($cm^3.mol^{-1}$)		$\mathcal{T}$	Residence time (s)
V	Volume (m^3)		δ	Membrane thickness (m)
x^*	Mole fraction of CO_2 in IL (-)		Ø	Packing fraction of Contactor (-)
y^*	Mole fraction of CO_2 in gas (-)		Υ	Surface tension ($mN\,m^{-1}$)

Subscripts

μ	Viscosity (cP)

1   Introduction

Carbon dioxide is believed as one of the major contributor to global warming and climate change (Figueroa et al., 2008). According to the reports of Intergovernmental Panel on Climate Change (IPCC), fossil fuels and minerals used for power generation contribute to almost 80 % of the total CO_2 emission (IPCC, 2005). The carbon level in the atmosphere can be controlled by capturing CO_2 from these power plants. Carbon capture, utilization and storage are emerging technologies used to manage CO_2 concentration through various techniques (Rahman et al., 2017; Yu et al., 2008). The three main technologies used for carbon capture are, post-combustion, pre-combustion and oxy-fuel combustion. Among these technologies, post-combustion can be easily implemented as it can be retrofitted to existing power plants (Chen et al., 2012; Qazi et al., 2020).

Membrane contactors are well known for membrane gas absorption operations. One of the main advantages of membrane contactor is its extremely high interfacial area which leads to process intensification due to reduction of the equipment size (Demontigny et al., 2005; Drioli et al., 2011; Falk-Pedersen et al., 2005; Li and Chen, 2005). Other advantages include, known and constant interfacial area, high operational flexibility, modularity and avoiding common problems of conventional absorption columns like flooding, foaming and channeling (Cui and Demontigny, 2013; Gabelman and Hwang, 1999; Mansourizadeh and Ismail, 2009). Major challenges faced in membrane contactors are wetting, fouling and degradation. Wetting can reduce the absorption performance due to significant increase in the mass transfer resistance inside the membrane (Mosadegh-Sedghi et al., 2014; Rangwala, 1996; Zhang et al., 2008). Wettability for the liquid absorbents is generally evaluated based on liquid entry pressure (LEP). LEP is the minimum pressure applied on the liquid to enter the membrane pores. To avoid wetting of the membrane, the transmembrane pressure should always be kept lower than the LEP (Franken et al., 1987; Zhao et al., 2016, 2015). Using hydrophobic membrane, composite membranes with dense skin layers and liquid absorbents of high surface tension can also reduce the risk of membrane wetting (Mosadegh-Sedghi et al., 2014). Fouling may be a critical concern while removing CO_2 from flue gases. To avoid fouling, pretreatment will be needed for flue gases to remove contaminants before entering the membrane contactor (Wang et al., 2014; Zhang et al., 2015). Membrane degradation can occur in the form of thermal and chemical degradation. Chemical solvents more likely degrade membranes (Barbe et al., 2000; Wang et al., 2004). Corrosive liquid absorbents can change the membrane morphology, hydrophobicity and chemical structures (Kladkaew et al., 2011).

Amino compounds like monoethanolamine (MEA), methyl diethanolamine (MDEA) and 2-amino-2-methyl-1-propanol (AMP) are commonly used absorbents for CO_2 (Kothandaraman, 2010; Qazi et al., 2019). Several drawbacks have been reported for CO_2 capture with amines, including high corrosion rate, high construction cost, and degradation by other component gases of the flue gas mixture as well as high energy consumption during regeneration (Yu et al., 2012). According to an estimate, almost 30 % of the energy of the power plant must be diverted for CO_2 capture process with amine solutions which nearly doubles the cost of electricity (Brennecke and Gurkan, 2010). Amine based CO_2 absorption involves chemical reaction with large amount of enthalpy which results in high energy demand for releasing the CO_2 in the regeneration step (Ramdin et al., 2012; Vaidya and Kenig, 2007). To replace these corrosive, volatile and degradation sensitive amines, ionic liquids (ILs) have been proposed as a special class of absorbents (Anthony et al., 2002; Blanchard et al., 1999). ILs are gaining attention due to their remarkable properties like high thermal stability, negligible volatility, high CO_2 solubility and tunable structures. The major advantage of ILs is their low volatility which results on more sustainable absorption processes when compared with classical absorption solvents (Rogers and Seddon, 2003). Moreover, their low vapor pressure result in low energy consumption for regeneration and CO_2 stripping. Thus, ILs can be regarded as promising alternative absorbents for energy and cost-efficient separation of CO_2 from industrial emissions.

Recently, many researchers have considered the combination of ILs with membrane contactors for CO_2 Capture. Luis et al. (2009) and Albo et al. (2010) used IL 1-ethyl-3-methylimidazolium ethylsulfate in a cross-flow membrane contactor to develop a zero solvent emission process concept. Gómez-Coma et al. (2014) and Albo and Irabien, (2012) used the same IL for non-dispersive absorption of CO_2 in parallel and cross flow membrane contactors. In their studies, effect of different process parameters, overall mass transfer coefficients and first order rate constant were systematically evaluated. Lu et al. (2014)

developed membrane absorption and desorption unit based on the ILs 1-butyl-3-methyl-imidazolium tetrafluoroborate ([bmim][BF$_4$]) (as physical absorbent) and 1-(3-aminopropyl)-3-methyl-imidazolium tetrafluoroborate ([apmim][BF$_4$]) (as chemical absorbent). Aqueous [apmim][BF$_4$] was able to give high CO$_2$ loading capacity even at atmospheric pressure. Aqueous [bmim][BF$_4$] was very easily regenerated at low cost compared to aqueous ([apmim][BF$_4$]. The author also investigated the membrane contactor absorption/desorption system for aqueous mixtures of ILs [bmim][BF$_4$] and [apmim][BF$_4$] with alkanolamine of 2-amino-2-methyl-1-propanol (AMP)(Lu et al., 2015). Results showed an enhanced transmembrane flux and loading capacity for ILs and AMP mixtures.

In this work, two room temperature ILs (RTILs), 1-ethyl-3-methylimidazolium methyl sulfate [emim][MS] and 1-ethyl-3-methylimidazolium dicyanamide [emim][DCA] were used as absorbents in a membrane contactor. These ILs have been reported as excellent CO$_2$ absorbents with high CO$_2$ solubility (Huang and Peng, 2017; Mejía et al., 2013; Yim et al., 2018) and low values of Henry's law constant. The reported Henry's law constant values for [emim][MS] and [emim]DCA were 7.1 MPa and 10.1 MPa, respectively (Sumon and Henni, 2011; Huang and Peng, 2017). The physical absorption nature of these RTILs makes it cost effective and energy saving during the desorption and regeneration process (Ramdin et al., 2012). Moreover, IL [emim][MS] and [emim]DCA] have high values of surface tension, contact angle and considerably moderate values of viscosity make these ILs very feasible for hydrophobic membrane contactor operations. Indeed, they have surface tensions of 63 mN m^{-1} and 60 mN m^{-1}, respectively (Klomfar et al., 2011; Santos and Baldelli, 2009). These values are very high compared to other ILs. Moderate viscosity values of 78.8 mPa s and 14.9 mPa s have been reported for [emim][MS] and [emim]DCA], respectively (Costa et al., 2011; Klomfar et al., 2011). The measured contact angles for the [emim][MS] and [emim]DCA] were 84.3° and 82.9°.

This work implements a comparatively new experimental and dynamic modelling approach for post-combustion carbon capture, by developing a coupled absorption/desorption membrane contactor setup and later expanding the study to a dynamic pseudo steady state modelling approach. The setup can either work in a single module absorption mode which only absorbs CO$_2$ in the membrane absorber or in a coupled absorption/desorption mode which allows to absorb CO$_2$ in the membrane absorber followed by the desorption in the membrane stripper within a single cycle. The coupled absorption/desorption mechanism provides interesting outcomes by integrating both absorption and desorption in a single step. Moreover, the study is based on pseudo steady state approach, that have never been thoroughly investigated both experimentally and in modelling. The ILs considered for this work have never been tested for membrane contactor absorption applications before, up to the author's knowledge. A mesoporous membrane contactor of parallel configuration and hydrophobic nature was selected, for the current study. CO$_2$ absorption/desorption behavior, CO$_2$ absorption capacity of RTILs, CO$_2$ removal efficiency of the membrane absorber, stripping efficiency of the membrane stripper, maximal CO$_2$ loading, CO$_2$ loading rate, mass transfer coefficients and enhancement factors were investigated here. For further development of the study, a dynamic pseudo steady state modelling approach was implemented to replicate the experimental findings by simulations and to perform parametric analysis and process optimization.

2   Experimental

2.1   Materials

Nitrogen gas of purity 99.9 % ±0.001 vol% and Carbon dioxide of purity 99.7 % ±0.01 vol% were purchased from Air Liquid Spain. ILs 1-ethyl-3-methylimidazolium methyl sulfate [emim][MS] and 1-ethyl-3-methylimidazolium dicyanamide [emim][DCA] were purchased from Sigma-Aldrich, with purity higher than 95 %. A polypropylene hollow fiber membrane contactor in parallel configuration was supplied by Liqui-Cel TM, USA. The module is of hydrophobic nature with mesoporous polypropylene hollow fibers of 40 % porosity and mean pore diameter of 0.04 µm, potted with polyurethane. Specifications of the membrane contactor are presented in table 1.

Table 1 Module specifications

Parameter	Value	unit
Membrane material	Polypropylene	-
Inner diameter of the fibers (d_i)	2.2 10^{-4}	m
Outer diameter of the fibers (d_o)	3.0 10^{-4}	m
Membrane thickness (δ)	0.4 10^{-4}	m
Length of the contactor (L)	0.115	m
Number of fibers (N)	2300	-
Membrane pore diameter(d_p)	0.04	µm
Effective inner membrane area (A)	0.18	m^2
Lumen side volume (V_g)	1.6 10^{-5}	m^3
Shell side volume (V_l)	2.5 10^{-5}	m^3
Porosity (ε)	40	%
Packing factor ($\emptyset$)	0.39	-
Tortuosity (τ)[a]	6.4	-

[a] $\tau = \dfrac{(2-\varepsilon)^2}{\varepsilon}$

2.2   Experimental setup

A membrane contactor setup suitable for CO_2 capture with ILs was developed here. As illustrated in figure 1, the setup is able to work in two modes; single module absorption and coupled absorption/desorption. In the single module absorption system, ILs were recirculated (in a closed loop) from the reservoir to the shell side of the membrane absorber. A digital gear pump (Cole-Parmer Gear Pump System, Benchtop Digital Drive, 0.017 mL/rev, 220 VAC, Spain) was used to maintain a constant flowrate and avoid fluctuations. In the coupled absorption/desorption system, ILs were recirculated (in a closed loop) at the same time through the shell side of both membrane absorber and membrane stripper. The feed gas mixture which contains CO_2 (15 % Vol.) and N_2 (rest to balance) was introduced through the lumen side of the membrane absorber. Feed gas flowrates (Q_g) were varied within the range of 10-50 ml min^{-1}. Single module absorption was investigated at two different levels of feed gas flow rates, 20 ml min^{-1} and 50 ml min^{-1}. Coupled/absorption desorption was investigated at three different levels of feed gas flow rates, 10 ml min^{-1}, 20 ml min^{-1} and 50 ml min^{-1}. The gas mixture was kept in open loop conditions with constant CO_2 concentration 15 % by Vol. Pure N_2 was allowed to pass from the lumen side of membrane stripper used as a sweep gas. Sweeping gas flowrate (Q_{N_2}) was always kept constant at 10 ml min^{-1}. Gas mass flowmeters (Alicat scientific, MC–gas mass flow controller, Spain) were used to measure and control the inflow and outflow of gases for both membrane absorber and membrane stripper. CO_2 concentration at the inlet and outlet of the membrane absorber and at the outlet of membrane stripper was analyzed by a CO_2 analyzer (Geotech,

G110 0-100%, UK). Liquid absorbent was introduced at an inlet pressure of 2.40 bar while gas was introduced at 1.03 bar. Liquid side pressure was always kept higher than the pressure of the gas side to avoid penetration of the gas into the liquid side. Although liquid side pressure was kept higher, however the transmembrane pressure was always controlled and kept below LEP to avoid wetting of the membrane. Wetting of the mesopores of membrane was not taken into account as fresh hydrophobic membranes were used with high surface tension ILs and experiments were performed under controlled transmembrane pressure (< LEP). Operating conditions are presented in table 2. Experimental setup was kept inside an oven to maintain isothermal conditions throughout the experiments. Gas flowmeters and gear measuring pumps were calibrated before experiments. ILs and gas streams were kept in countercurrent arrangements in both membrane absorber and stripper.

In the single module absorption, IL recirculates in a closed loop, through the shell side of the membrane absorber. The gas flows in an open loop through the lumen side, without any recirculation. Continuous recirculation of the IL allows absorbing CO_2 from the gas mixture, which accumulates on the liquid side. The absorption rate and accumulation of CO_2 on the liquid side slows down with time and reaches a pseudo steady state, where the absorption rate becomes nearly constant. The evolution of CO_2 concentration at the gas side outlet was continuously monitored with CO_2 analyzer. After reaching pseudo steady state, the CO_2 desorption/stripping was initiated in the same module which was used as a stripper having N_2 as sweep gas. IL was kept recirculating in the closed loop desorbing CO_2 into the pore of mesoporous membrane. In the coupled absorption/desorption, simultaneous absorption and desorption were carried out in a single step. IL liquid during recirculation, first passes from membrane absorber absorbing CO_2 and after enters the membrane stripper having N_2 as sweep gas to desorb CO_2 in the same step. CO_2 concentration at the gas side outlet of membrane absorber and stripper were continuously monitored with CO_2 analyzer. The pseudo steady state was achieved like on the single module absorption. During continuous recirculation of IL (in a closed loop), CO_2 was absorbed and accumulated (on liquid side) in the absorption module a part of which desorbs after entering the stripping module. The IL was recirculated, until a constant CO_2 concentration was achieved at the gas side outlet (reaching pseudo steady state). All the experiments were repeated and reproduced three times. The data presented in the manuscript represents the average values for the set of three experiments.
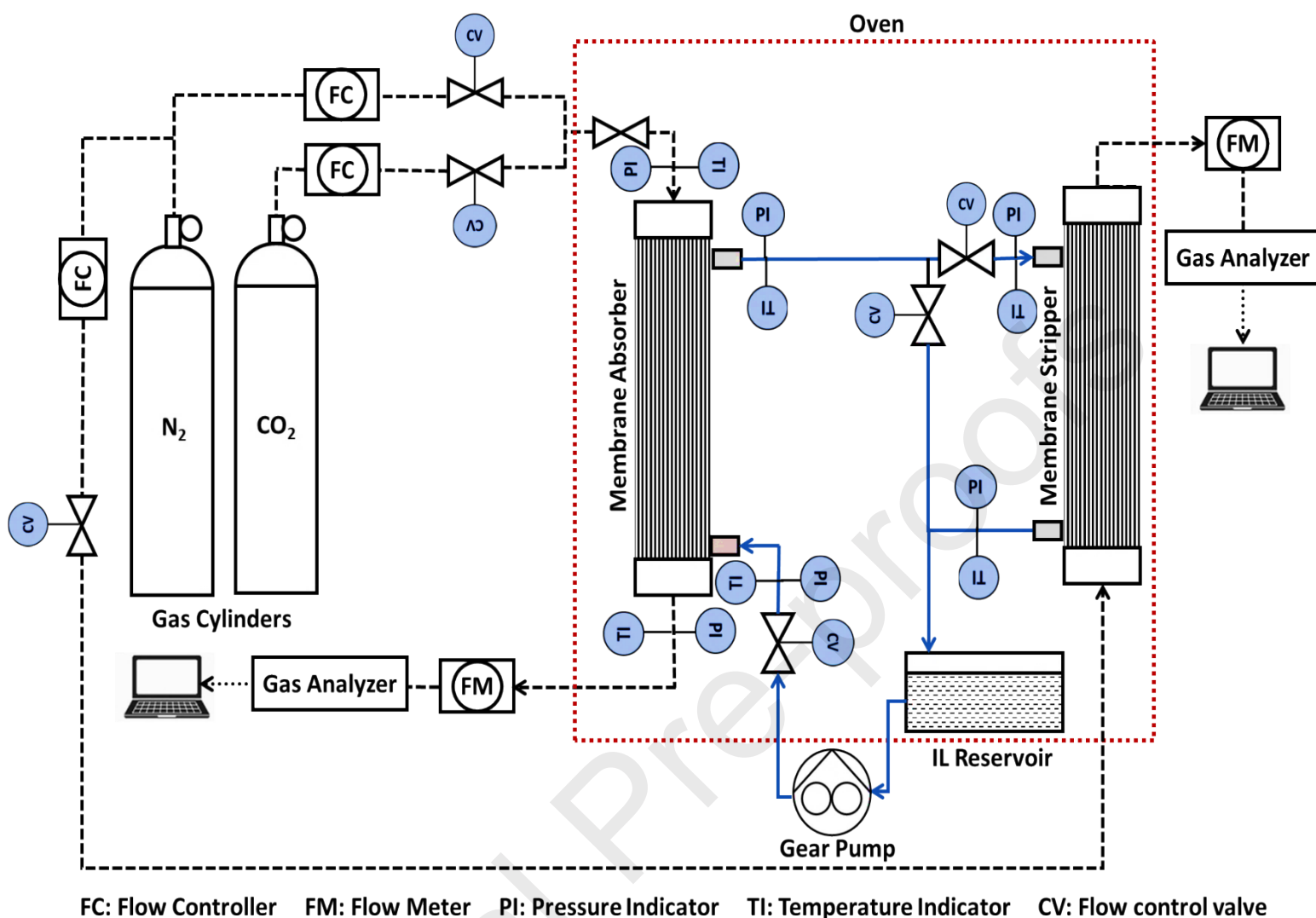
Figure 1 Schematic representation of the experimental setup; Gas flow (black dashed lines), Liquid flow (solid blue lines).

Table 2 Operating conditions

Parameter/Property Description	Value	Unit
Ionic liquids	[emim] [MS] ≥ 95%	-
	[emim] [DCA] ≥ 95%	-
CO_2 concentration	15	Vol %
Temperature, T	288	K
Sweeping gas flowrate, Q_{N_2}	100	ml min^{-1}
Feed gas flowrate, Q_g,	10-50	ml min^{-1}
Liquid flowrate, Q_l	60	ml min^{-1}
Gas inlet pressure, $P_{g,in}$	1.03	Bar
Liquid inlet pressure, $P_{l,in}$	2.40	Bar
LEP [a], [emim] [MS]	2.40	Bar
LEP [a], [emim] [DCA]	2.81	Bar

[a] $LEP = \Delta P = -\frac{4B \Upsilon \cos \theta}{d_{max}}$; B − pore geometry coefficient,

Υ − surface tension, θ − contact angle, d_{max} − maximum pore diameter

3 Theory

3.1 Mass transfer Kinetics

Performance of CO_2 capture with ILs in both single module absorption and coupled absorption/desorption system were evaluated based on membrane flux j_{CO_2}, experimental mass transfer coefficient K_{exp}, liquid CO_2 loading α and enhancement factor E. Membrane flux can be calculated as below.

$$j_{CO_2} = \frac{1}{A}\left(\frac{d\tilde{n}}{dt}\right) = \frac{Q_{g,in}\,C_{g,in} - Q_{g,out}\,C_{g,out}}{A} = K_{exp}\,\Delta C_{g,lm} \tag{1}$$

Where ñ represents moles of CO_2, $C_{g,in}$ and $C_{g,out}$ are gas side inlet and outlet concentrations ($mol\ m^{-3}$) of CO_2, $Q_{g,in}$ and $Q_{g,out}$ are gas side inlet and outlet flow rates ($m^3\ s^{-1}$), respectively. The logarithmic mean of the driving force $\Delta C_{g,lm}$ can be calculated using the equation below.

$$\Delta C_{g,lm} = \frac{(C_{g,in} - C_{g,in}^*) - (C_{g,out} - C_{g,out}^*)}{\ln\left(\frac{C_{g,in} - C_{g,in}^*}{C_{g,out} - C_{g,out}^*}\right)} \tag{2}$$

Where $C_{g,in}^*$ and $C_{g,out}^*$ in above equation are concentrations of the gas phase in equilibrium with the corresponding CO_2 concentration in the liquid phase C_l^*. Equilibrium concentration of gas phase C_g^* can be found using the equation presented below (Luis et al., 2009; Sander, 2015).

$$H_d = \frac{C_g^*}{C_l^*} = \frac{y^*\rho_g}{x^*\rho_l} = \frac{y^*}{x^*\rho_l}\frac{P_T}{\tilde{R}T} \tag{3}$$

Where y^* and x^* are equilibrium mole fractions of CO_2 in gas and liquid phase, respectively, P_T is the total pressure and ρ_l represents molar density ($mol\ L^{-1}$) of the liquid.

Assuming no-wetting conditions for a membrane contactor having gas on lumen side and liquid on the shell side, the resistance in series approach considering enhancement due to chemical reaction can be written as below (Ortiz et al., 2010).

$$\frac{1}{K_{ov}} = \frac{d_o}{k_g d_i} + \frac{d_o}{k_m d_{lm}} + \frac{1}{k_l H_d E} \tag{4}$$

By neglecting contributions of the gas and membrane phase (considering non-wetting conditions and gas filled membrane pores) and replacing experimental overall mass transfer coefficient, K_{exp} calculated from equation 1 by K_{ov}, equation 4 can be rewritten for enhancement factor as under;

$$E = \frac{K_{exp}}{k_l H_d} \tag{5}$$

For shell side liquid mass transfer coefficient in parallel flow membrane contactor, the correlation developed by Li et al. has been used in this study as it closely meets the conditions of current absorption process (Shen et al., 2010).

$$Sh = \left(\frac{k_l d_h}{D_l}\right) = (0.52 - 0.64\emptyset)R_e^{(0.36 + 0.3\emptyset)}S_c^{0.33} \text{ for } 0 < R_e < 100 \text{ and } 0.30 < \emptyset < 0.70 \tag{6}$$

While hydraulic diameter d_h, packing fraction of membrane contactor $\emptyset$, Reynolds number R_e and Schmidt number S_c, can be calculated according to the equations presented in appendix A. CO_2

diffusivity in liquid phase D_l can be predicted by correlation developed by Morgan et al. (2005), for imidazolium based ILs.

$$D_l = 2.66 \; 10^{-3} \frac{1}{\mu_{IL}^{0.66} v_{CO_2}^{1.04}}$$ (7)

3.2 Modelling approach

A dynamic modelling approach was implemented here for the process explained in section 2.2. Characteristics of the membrane module considered for membrane absorber and membrane stripper were adopted from table 1. Operating conditions were implemented according to the table 2. Properties of the ILs used in the model are presented in table 3. The assumptions considered for hydrodynamics and thermodynamics of the model are; (1) Pseudo steady state (recirculation of IL in closed loop) and isothermal conditions. (2) Countercurrent arrangements for gas and IL flow in membrane absorber and membrane stripper. (3) Fully developed Laminar velocity profile in the tube and shell. (4) Application of Henry's law on gas-liquid interface. (5) Non-wetted conditions of membrane with no selectivity. (6) Fick's diffusion through porous media of membrane and neglecting convective contributions. (7) Considering contributions of advection and diffusion to mass balance based on local concentrations. (8) Perfectly stirred liquid absorbent tank.

3.2.1 Model equations

The continuity equation based on the above-mentioned assumptions can be written as below.

$$-\nabla . C_i U = \frac{\partial C_i}{\partial t} + \nabla . j_i$$ (8)

Where $C_i (mol \; m^{-3})$, $U \; (m \; s^{-1})$ and $j_i \; (mol \; m^{-2} \; s^{-1})$ represents concentration of the solute, velocity of the specie and mass transfer flux, respectively. For the tube (gas), membrane (gas filled pores) and shell (liquid), the above equation is written as below.

$$U_{z,g-A} \frac{\partial C_{g-A}}{\partial z} = \frac{\partial C_{g-A}}{\partial t} + D_{g-A} \left[\frac{\partial^2 C_{g-A}}{\partial r^2} + \frac{1}{r} \frac{\partial C_{g-A}}{\partial r} + \frac{\partial^2 C_{g-A}}{\partial z^2} \right]; U_{z,g-S} \frac{\partial C_{g-S}}{\partial z} = \frac{\partial C_{g-S}}{\partial t} + D_{g-S}$$

$$\left[\frac{\partial^2 C_{g-S}}{\partial r^2} + \frac{1}{r} \frac{\partial C_{g-S}}{\partial r} + \frac{\partial^2 C_{g-S}}{\partial z^2} \right]$$ (9)

$$0 = \frac{\partial C_{m-A}}{\partial t} + D_{m-A} \left[\frac{\partial^2 C_{m-A}}{\partial r^2} + \frac{1}{r} \frac{\partial C_{m-A}}{\partial r} + \frac{\partial^2 C_{m-A}}{\partial z^2} \right]; \qquad 0 = \frac{\partial C_{m-S}}{\partial t} + D_{m-S} \left[\frac{\partial^2 C_{m-S}}{\partial r^2} + \frac{1}{r} \frac{\partial C_{m-S}}{\partial r} + \frac{\partial^2 C_{m-S}}{\partial z^2} \right]$$

(10)

$$U_{z,l-A} \frac{\partial C_{l-A}}{\partial z} = \frac{\partial C_{l-A}}{\partial t} + D_{l-A} \left[\frac{\partial^2 C_{l-A}}{\partial r^2} + \frac{1}{r} \frac{\partial C_{l-A}}{\partial r} + \frac{\partial^2 C_{l-A}}{\partial z^2} \right]; U_{z,l-S} \frac{\partial C_{l-S}}{\partial z} = \frac{\partial C_{l-S}}{\partial t} + D_{l-S}$$

$$\left[\frac{\partial^2 C_{l-S}}{\partial r^2} + \frac{1}{r} \frac{\partial C_{l-A}}{\partial r} + \frac{\partial^2 C_{l-A}}{\partial z^2} \right]$$

(11)

The subscripts A and S represents membrane absorber and membrane stripper, respectively. Fully developed velocity profile of the gas on lumen side was predicted by Hagen-Poiseuille equation with no slip conditions, while for the velocity on shell side Happel's free surface model was used (Happel, 1959).

$$U_{z,g-A} = 2u_{g-A}\left[1 - \left(\frac{r}{r_1}\right)^2\right]; \quad U_{z,g-S} = 2u_{g-S}\left[1 - \left(\frac{r}{r_1}\right)^2\right] \tag{12}$$

$$U_{z,l-A} = U_{z,l-S} = 2u_l\left[1 - \left(\frac{r_2}{r_3}\right)^2\right]\frac{\left(r/r_3\right)^2 - \left(r_2/r_3\right)^2 + 2\ln\left(r_2/r\right)}{3 + \left(r_2/r_3\right)^4 - 4\left(r_2/r_3\right)^2 + 4ln\left(r_2/r_3\right)}; \quad r_3 = r_2\sqrt{\frac{1}{1-\emptyset}}; \quad 1 - \emptyset = \frac{Nr_2^2}{r_{c,i}^2}$$

(13)

Where r_1 and r_2 represents inner and outer radius of the fiber, r_3 represents radius of the arbitrary shell around the fiber and $r_{c,i}$ represents inner radius of the contactor.

Diffusivity of CO_2 and N_2 in the gas phase (D_g) was measured by correlation developed by Fuller et al. (1966), while for CO_2 diffusivity in ionic liquid (D_l), the diffusivity correlation developed by Morgan et al. (2005) was used, which is presented as equation 7 in preceding section. Diffusivity of CO_2 and N_2 inside the membrane (D_m), was considered as combined effects of gas diffusivity, D_g and Knudsen diffusivity D_{Kn}.

$$D_g = \frac{0.01013.T^{1.75}\left(\frac{1}{M_{CO_2}} + \frac{1}{M_{N_2}}\right)^{0,5}}{P\left[\left(\Sigma\bar{\upsilon}_{CO_2}\right)^{\frac{1}{3}} + \left(\Sigma\bar{\upsilon}_{N_2}\right)^{\frac{1}{3}}\right]^2} \tag{14}$$

$$\frac{1}{D_m} = \frac{1}{D_g} + \frac{1}{D_{Kn}} \tag{15}$$

Details of the gas diffusivity D_g and Knudsen diffusivity D_{Kn} are presented in appendix B.

A transient state differential equation was applied across the reservoir to measure the evolution of CO_2 concentration in the IL reservoir.

$$V_{IL}\frac{dC_{\check{r}(t)}}{dt} = Q_{IL}\left(C_{\check{r},in}(t) - C_{\check{r},out}(t)\right) \tag{16}$$

Where $C_{\check{r}}$ in equation 16 represents the concentration of CO_2 in the IL reservoir. Final form of the equation can be as;

$$C_{\check{r},out}(t + \Delta t) = \frac{\Delta t}{\mathcal{T}_{IL}}C_{\check{r},in}(t) + C_{\check{r}}(t)\left[1 + \frac{\Delta t}{\mathcal{T}_{IL}}\right], \quad C_{\check{r},in}(t) = \frac{\iint_{r=r_2}^{r=r_3}C_l(r)rdrd\theta}{\iint_{r=r_2}^{r=r_3}rdrd\theta}, \quad \mathcal{T}_{IL} = \frac{V_{IL}}{Q_{IL}} \tag{17}$$

The term $C_{\check{r},out}(t + \Delta t)$ in the above equation represents the outlet concentration of the reservoir at time $t + \Delta t$. Properties of the ILs and parameters used in the model are presented in table 3.

Table 3 Properties of the Ionic Liquids and Parameters for model

Property	Value	Reference
Viscosity: μ (**mPa s**); **298 K**		
[emim][MS]	78.8	(Costa et al., 2011)
[emim][DCA]	14.9	(Quijada-Maldonado et al., 2012)
Density: ρ (**g cm^{-3}**); **298 K**		
[emim][MS]	1.282	(Costa et al., 2011)
[emim][DCA]	1.102	(Quijada-Maldonado et al., 2012)

Surface Tension : γ (mN m^{-1}) ; 298 K		
[emim][MS]	63	(Santos and Baldelli, 2009)
[emim][DCA]	60	(Klomfar et al., 2011)
Contact Angle (Deg)		
[emim][MS]	84.3	This work
[emim][DCA]	82.9	This work
Diffusivity of CO$_2$ in ILs: D$_l$ (cm^2 s^{-1}), 298 K		
[emim][MS]	3.88 10^{-6}	This work
[emim][DCA]	1.16 10^{-5}	This work
Henry's law constant: H (MPa), 298K		
[emim][MS]	7.1	(Sumon and Henni, 2011)
[emim][DCA]	10.1	(Huang and Peng, 2017)

3.2.2 Meshing, boundary conditions and numerical resolution

Figure 2(a) represents schematic representation of the pseudo steady state setup for gas absorption/desorption in a membrane contactor. Gas enters inside the lumen of the membrane at z=0 and exits at z=L, while IL, which recirculates through the shell side, enters at z=L and exits at z=0. For reasonable computing time, a single hollow fiber was considered for modeling. A portion of the fiber and the arbitrary shell (r$_3$), to be modeled, are presented in figure 2 (b). Figure 2 (b) represents the two-dimensional meshed geometry of the tube, membrane and shell, considered for modelling. Length of the fiber is represented by L, while radius of the tube, membrane and shell are represented by r$_1$, r$_2$ and r$_3$, respectively. A refined mapped mesh was applied (in COMSOL Multiphysics®) across the three domains of the current symmetrical geometry. More refined mesh was selected inside the mesoporous membrane. Selecting an appropriate mesh for the finite element analysis is very critical. A rigorous absorption model with sufficient discretization (particularly in radial direction) of the liquid (due to high resistance for mass transfer) and membrane phase (due to high resistance for mass transfer and existence of interface) are required. The rectangular meshing elements are in accordance with the two directional (r, z) mass transport.

Boundary conditions (BCs) required for solving the model equations are labeled in figure 2(b). Details of the labeled BCs for both membrane absorber and membrane stripper are listed in table 4 below.
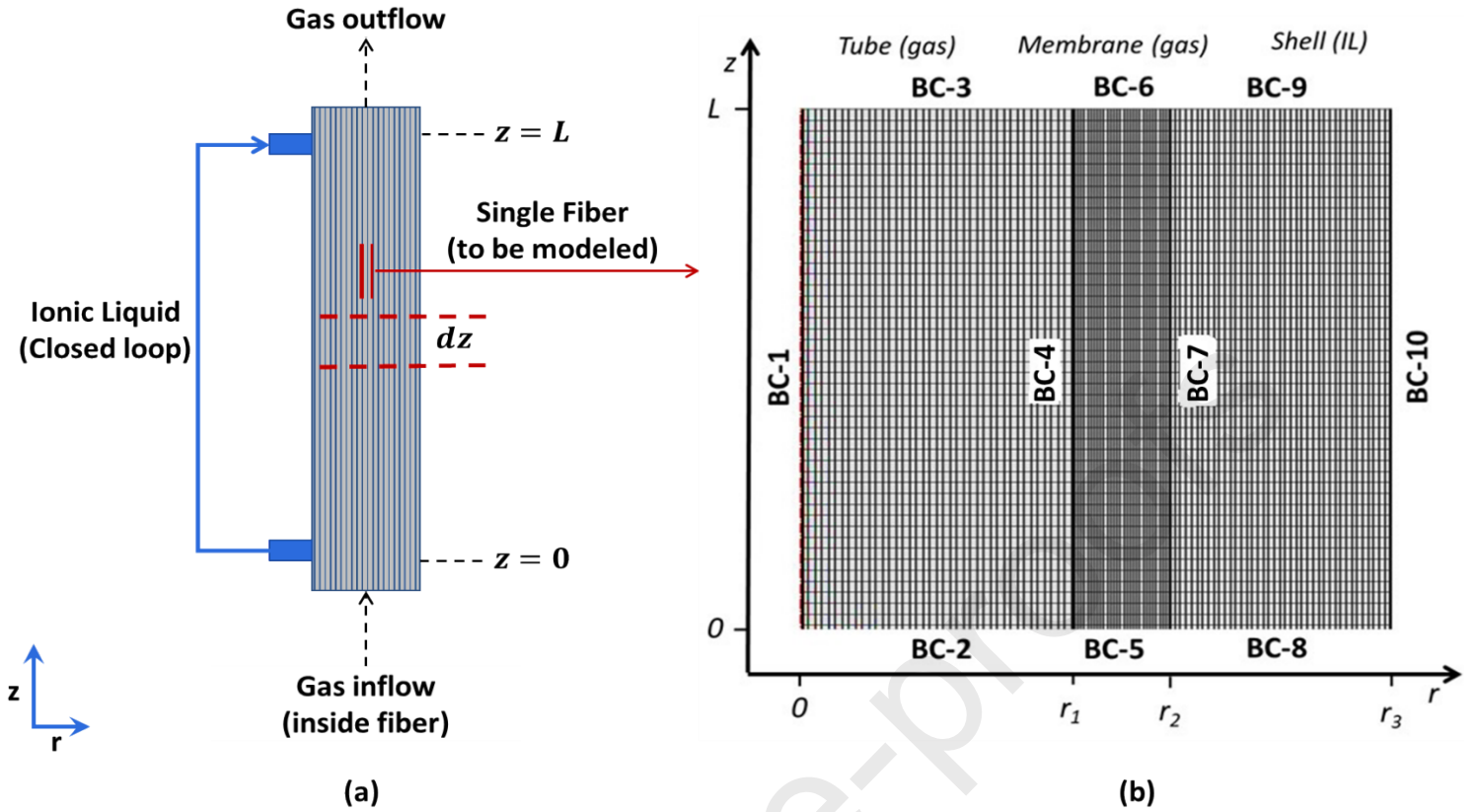
(a) **(b)**

Figure 2 (a) Schematic representation of the pseudo steady state setup for gas absorption/desorption in a membrane contactor, (b) Two-dimensional meshed domains (tube, membrane and shell) and boundaries of the membrane absorber and membrane stripper.

Table 4 Boundary conditions for the dynamic 2-D model

Boundary	Condition	Membrane absorber	Membrane stripper
$BC-1$	Axial symmetry	$\dfrac{\partial C_{g-A}}{\partial r} = 0$	$\dfrac{\partial C_{g-S}}{\partial r} = 0$
$BC-2$	Inlet gas conditions	$C_{g-A} = C_{g-A,\,in}$	$C_{g-S} = C_{g-S,\,in}$
$BC-3$	Convective flux at gas outlet	$-D_{g-A}\dfrac{\partial C_{g-A}}{\partial z} = 0$	$-D_{g-S}\dfrac{\partial C_{g-S}}{\partial z} = 0$
$BC-4$	Interfacial continuity	$C_{g-A} = C_{m-A}$	$C_{g-S} = C_{m-S}$
$BC-5$	No Flux	$-D_{m-A}\dfrac{\partial C_{m-A}}{\partial z} = 0$	$-D_{m-S}\dfrac{\partial C_{m-S}}{\partial z} = 0$
$BC-6$	No Flux	$-D_{m-A}\dfrac{\partial C_{m-A}}{\partial z} = 0$	$-D_{m-S}\dfrac{\partial C_{m-S}}{\partial z} = 0$
$BC-7$	Interfacial gas liquid equilibrium	$C_{l-A} = H_d C_{m-A}$	$C_{m-S} = H_d C_{l-S}$
$BC-8$	Convective flux at liquid outlet	$-D_{l-A}\dfrac{\partial C_{l-A}}{\partial z} = 0$	$-D_{l-S}\dfrac{\partial C_{l-S}}{\partial z} = 0$
$BC-9$	Inlet liquid conditions	$C_{l-A} = C_{\check{r},out}(t + \Delta t)$	$C_{l-S} = C_{l-A,out}$
$BC-10$	Axial symmetry	$\dfrac{\partial C_{l-A}}{\partial r} = 0$	$\dfrac{\partial C_{l-S}}{\partial r} = 0$

Equations presented in section 3.2.1 were solved using COMSOL Multiphysics® (version 5.3a, 2018) and MATLAB R2017a using LiveLink™ for MATLAB®. The model predicts dependent variables of mass transport equations ($C_i (mol.m^{-3})$ and $U\ (ms^{-1})$), momentum transport equations ($U\ (ms^{-1})$) and differential mass balance over reservoir ($C_{\dot{r},out}(t + \Delta t)$). Finite element method was implemented here. This method considers piecewise polynomial interpolation over the domains and numerically resolves equations at each of the nodes. Fully coupled solver settings were applied for BDF time stepping and strict steps were implemented for the solver. To avoid a high number of elements in the axial direction and reduce the large difference between r and z directions, the 2D equation system was scaled down axially. An axial scale factor was applied on the axial coordinate, fiber length, diffusion coefficients and interstitial velocities.

4   Results and discussion

4.1   CO$_2$ absorption/desorption

The absorption performance of CO$_2$ in two different 1-ethyl-3-methyl imidazolium based ILs, in single module absorption setup and coupled absorption/desorption setup, are presented here in terms of efficiency and CO$_2$ loadings. The CO$_2$ removal efficiency in the membrane absorber was found using the following expression.

$$CO_2\ removal\ efficiency\ (\%) = \left(1 - \frac{C_{g,out}}{C_{g,in}}\right)100 \tag{18}$$

Where $C_{g,in}$ and $C_{g,out}$ represents inlet and outlet concentrations of CO$_2$ for the membrane absorber.

Figure 3 below represents the CO$_2$ removal efficiencies of ILs [emim][MS] and [emim][DCA] in the membrane absorber, for the experimental setup presented in section 2.2 against operation time. The efficiencies for both single module absorption and coupled absorption/desorption at various feed gas flow rates (of membrane absorber) are reported here to study and compare. ILs were able to achieve nearly 100 % efficiency in the beginning of the operation. During recirculation of the single module absorption, IL absorbs CO$_2$ inside membrane absorber which leads to the accumulation of CO$_2$ in the liquid side and hence the efficiency decreases with the operation time. After enough recirculations, the absorption process reaches pseudo steady state, where the absorption rate becomes nearly constant (constant CO$_2$ removal efficiency). When coupled absorption/desorption is considered, the IL during a single cycle absorbs (passing from membrane absorber) and desorbs (passing from membrane stripper) CO$_2$. As can be seen from figure 3, even after 70 minutes of operation, the coupled process retained a very high efficiency of 82 % and 66 %, for IL [emim][MS] and [emim][DCA], respectively. IL [emim][MS] at 20 ml min^{-1} feed gas flowrate retained pseudo steady state efficiencies of 65 % and 11 % for coupled absorption/desorption and single module absorption, respectively. IL [emim][DCA] at 20 ml min^{-1} feed gas flowrate showed pseudo steady state efficiencies of 59 % and 17 % for coupled absorption/desorption and single module absorption, respectively. Gómez-Coma et al. (2014) in their studies, used IL [emim][ESO$_4$] in a single module absorption and has reported nearly 10 % efficiency for feed gas flowrate of 70 ml min^{-1}. By comparing efficiency of their studies with the efficiencies of the current coupled absorption/desorption at 20 ml min^{-1}, a difference of 37 % and 31 % was observed, for [emim][MS] and [emim][DCA], respectively. In another study, the author has reported to achieve 20.4 % experimental efficiency and 20.9 % simulation efficiency, for IL [emim][Ac], which is far lower than the efficiency achieved for current coupled absorption/desorption system (Gómez-Coma et al.,

2017). Other studies have reported better absorption performances with reactive ILs and conventional absorbents (Lu et al., 2014, 2013; Makhloufi et al., 2014), however those absorbents have several drawbacks which have been discussed in preceding sections. In fact, the main advantage of using room temperature ILs (which behaves as physical absorbents) for the current coupled absorption/desorption is in the effective stripping and ease of regeneration of the absorbent compared to other absorbents, which makes them very cost effective.
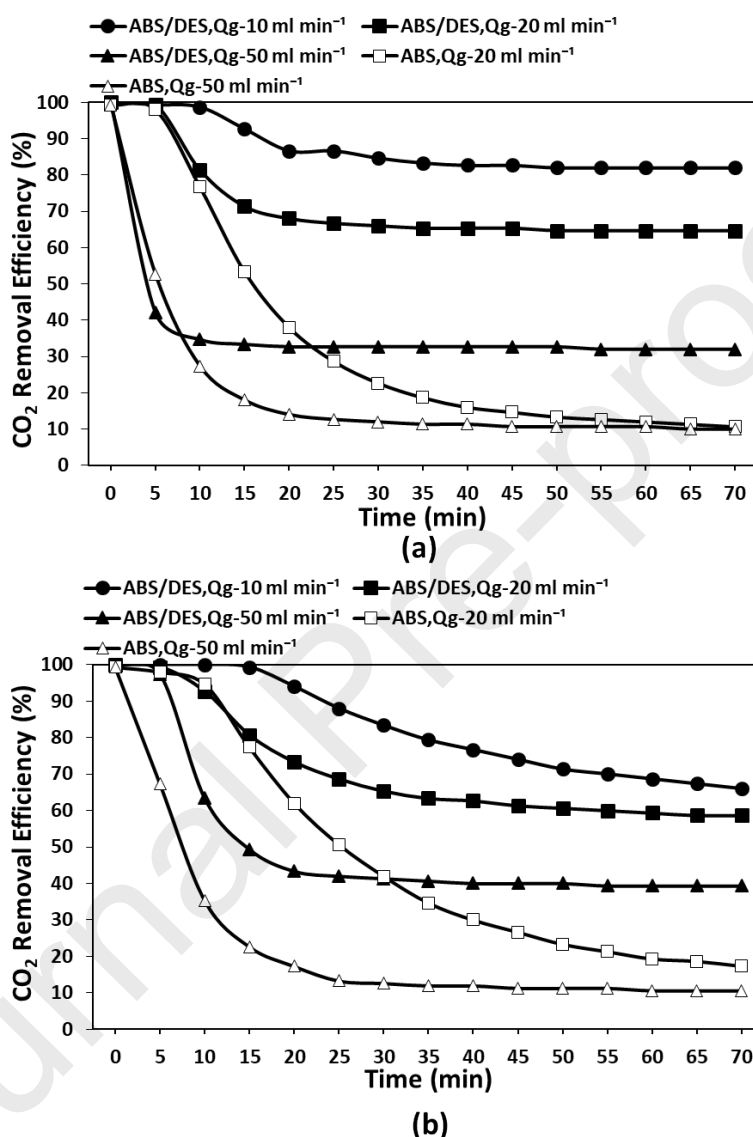
Figure 3 CO_2 removal efficiency of the membrane absorber for coupled absorption/desorption (ABS/DES) and single module absorption (ABS) against operation time for IL (a) [emim] [MS] and (b) [emim] [DCA]

As mentioned above, considering feed gas flowrate of 10 ml min^{-1} for coupled absorption/desorption process, ILs [emim][MS] and [emim][DCA] shows 82 % and 66 % efficiency. The rest of 18 % and 34 % CO_2 remains absorbed and cannot be desorbed in single cycle having same operating conditions. The above-mentioned results explain the very physical absorption nature of the RTILs [emim][MS] and [emim][DCA]. Retaining very high absorption efficiencies for coupled process with RT sweep desorption, shows the ease of desorption of CO_2 from RTILs compared to that of conventional absorbents, which require a huge amount of heat and energy to desorb CO_2.

Feed gas flowrate has shown significant effect on the CO_2 removal efficiencies, particularly for Coupled process. For IL [emim][Ms], increasing gas flowrate from 10 ml min^{-1} to 50 ml min^{-1}, decreases CO_2 removal efficiency by 50 %. For [emim][DCA], the same increase in gas flow flowrate decreases CO_2 removal efficiency by 27 %. Increase in gas flowrate has two significant effects; a decrease in the residence time of gas inside the membrane absorber and increase in mass transfer flux across the interface. This increase in mass transfer flux also causes high CO_2 loading, which again negatively affects the absorption performance of absorbents.

The increase in CO_2 loading with the operation time is presented in figure 4. A huge difference of 4.6 10^{-3} mol mol^{-1} and 4.8 10^{-3} mol mol^{-1} can be observed, for ILs [emim][MS] and [emim][DCA], respectively, between the loadings of single module absorption and coupled absorption/desorption. At feed gas flowrate of 20 ml min^{-1}, after 70 minutes of recirculation, CO_2 loading reaches 1 10^{-3} mol mol^{-1} and 5.6 10^{-3} mol mol^{-1} for coupled absorption/desorption and single module absorption, respectively, while using IL [emim][MS] as an absorbent. For IL [emim][DCA], at feed gas flowrate of 20 ml min^{-1}, CO_2 loading reached 2.7 10^{-3} mol mol^{-1} and 7.5 10^{-3} mol mol^{-1}, for coupled absorption/desorption and single module absorption, respectively, after 70 minutes of recirculation of the IL. An initial faster increase in the CO_2 loading can be observed, which later slows down with time. The initial faster loading can be attributed as result of interfacial absorption, which later slows down when the absorption is transferred toward the bulk of the IL (Low diffusion coefficients causes high mass transfer resistance). Initially, the CO_2 loading rate drops with time due to the accumulation of CO_2 on the liquid side until it reaches the pseudo steady state. At pseudo steady state, the absorption rate and thus the CO_2 loading rate becomes nearly constant. After this stage, a constant amount of CO_2 is accumulated with further recirculation.

Maximal CO_2 loading at pseudo steady state is presented in figure 5. Effect of feed gas flowrate on the CO_2 can be observed from the figure. A higher feed gas flowrate has increased the CO_2 loading. For [emim][MS], in case of single module absorption, increase in feed gas flowrate from 20 ml min^{-1} to 50 ml min^{-1} increases CO_2 loading from 5.8 10^{-3} mol mol^{-1} to 9 10^{-3} mol mol^{-1}. For coupled absorption/desorption, an increase from 1 10^{-3} mol mol^{-1} to 1.8 10^{-3} mol mol^{-1} was observed by increasing feed gas flowrate from 20 ml min^{-1} to 50 ml min^{-1}. A very low CO_2 loading was retained during absorption desorption operation of RTILs. IL [emim][MS] at pseudo steady state, 50 ml min^{-1} feed gas flowrate and coupled absorption/desorption operation, keeps nearly a constant CO_2 loading of 1.8 10^{-3} mol mol^{-1}, which for single module absorption was 9 10^{-3} mol mol^{-1}. For [emim][DCA] at the same operating conditions, CO_2 loadings of 4.8 10^{-3} mol mol^{-1} and 9.4 10^{-3} mol mol^{-1} were observed for coupled absorption/desorption and single module absorption, respectively. The above-mentioned differences between the CO_2 loadings of coupled absorption/desorption and single module absorption, confirms the physical absorption nature and ease of CO_2 desorption of these RTILs. Moreover, the RT sweep desorption was much more efficient for [emim][MS] compared to [emim][DCA], as the later IL retained nearly double CO_2 loading at pseudo steady state.
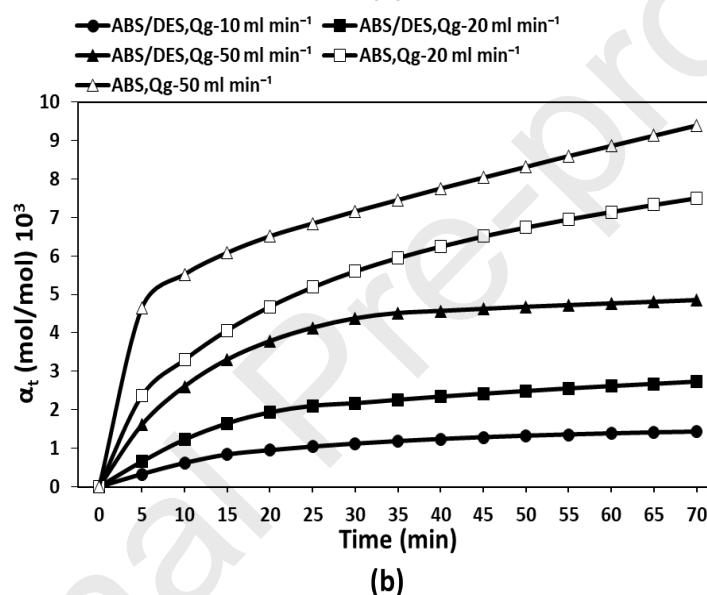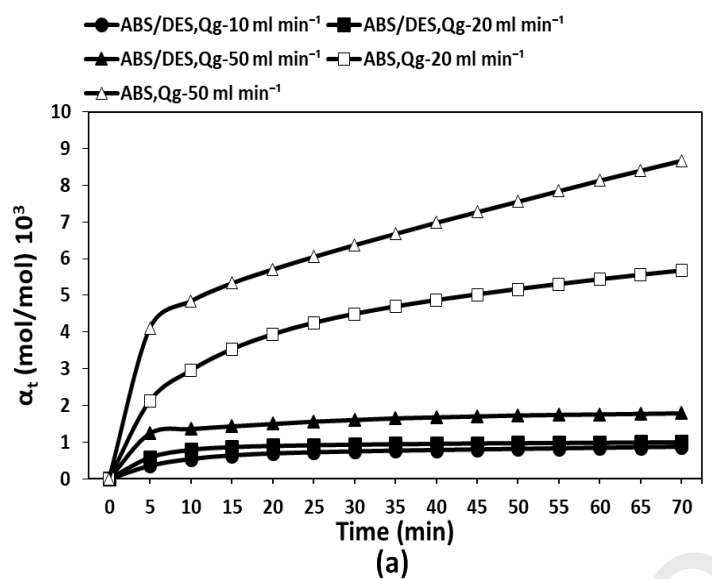
Figure 4 CO_2 loading α_t of the IL (a) [emim] [MS] and (b) [emim] [DCA] during coupled absorption/desorption (ABS/DES) and single module absorption (ABS) against operation time
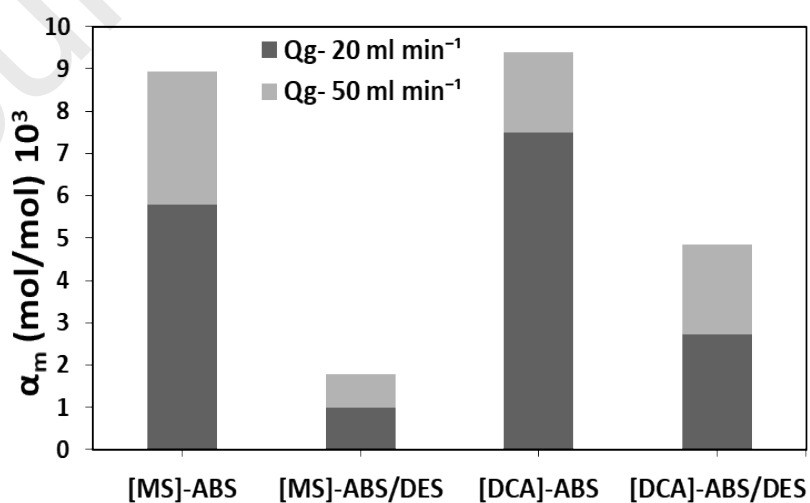
Figure 5 Maximal CO_2 loading, α_m, of the ILs [emim] [MS] ([MS]) and [emim] [DCA] ([DCA]) during coupled absorption/desorption (ABS/DES) and single module absorption (ABS) after 70 minutes of operation

As explained in the experimental section, in the coupled process the IL in a single recirculation step absorbs CO_2 in the membrane absorber and desorbs it in the membrane stripper. The stripping efficiency of the RTILs in the membrane stripper is presented here. The CO_2 stripping efficiency was found from the following equation.

$$Stripping\ efficiency\ (\%) = \left(1 - \frac{C_{l,out}}{C_{l,in}}\right)100 \qquad (19)$$

Where $C_{l,in}$ and $C_{l,out}$ represents CO_2 concentrations of the IL at inlet and outlet of the membrane stripper.

Stripping efficiency of the CO_2 in the membrane stripper during coupled absorption/desorption operation against operation time is presented in figure 6. The stripping gas flowrate was always kept constant at 100 ml min^{-1}. Feed gas flowrate in membrane absorber was varied from 20 ml min^{-1} to 50 ml min^{-1}. A considerable effect of feed gas flowrate on the striping efficiency can be observed. A higher stripping efficiency was achieved at lower feed gas flow rate. This effect might be due to the lower CO_2 loading at lower feed gas flowrates which increases the stripping efficiency due to the presence of less amount of CO_2 to be desorbed. Another important phenomenon, which can be observed from the figure 6 below, is the very low initial efficiency which increases with time and nearly reaches to a constant value at pseudo steady state. Initially, [emim][Ms] achieves a stripping efficiency of 18 % at 20 ml min^{-1} feed gas flowrate, which increases up to 86 % at pseudo steady state. IL [emim][DCA] was able to achieve only 4 % initial efficiency at the same operating conditions, which reaches 65 % at pseudo steady state. Initially the absorption behaves more like interfacial chemical in nature and the sweep gas stripping was not much efficient. The interfacial faster absorption is not effective at higher concentrations of CO_2 in the IL. Thus, the absorption later adopts the physical absorption nature and shifts to the bulk of the IL. Sweep gas stripping becomes much efficient for the physically absorbed CO_2 in the RTILs and nearly reaches 86 % for [emim][Ms]. It can also be observed that stripping was much more efficient for IL [emim][Ms] than [emim][DCA]. IL [emim][Ms] was able to achieve very high stripping efficiency (from 18%-86%) compared to [emim] [DCA] (from4%-65 %).

The comparatively very high stripping efficiencies of 86 % and 65 %, for the ILs [emim][Ms] and [emim][DCA], respectively, represents the easy and cost-efficient regeneration potential of these absorbents, compared to reactive ILs and other conventional absorbents. A simulation study has reported 16 % reduction in the energy loss and 12 % reduction in the equipment footprint for CO_2 capture with the IL [bmim][Ac] instead of using MEA (Shiflett et al., 2010). Lu et al. (2014) investigated, room temperature IL [bmim][BF$_4$] (physical absorbent) and task specific IL [apmim][BF4] (reactive absorbent) for vacuum regeneration in a membrane contactor. Even at very low vacuum level, IL [bmim][BF$_4$] showed nearly 100 % regeneration efficiency. CO_2 loading of the IL [bmim][BF$_4$] rapidly decreased and reached almost zero in 26 minutes. IL [apmim][BF$_4$] could not be completely regenerated, even after 55 minutes of operation. No further regeneration was possible after this time, and a constant CO_2 loading was observed, even at high vacuum levels. It was concluded that [bmim][BF$_4$] due to its physical absorption nature is an energy saving absorbent of CO_2. More intensive

regeneration techniques were recommended such as hot regeneration, to completely regenerate [apmim][BF$_4$], which makes it very costly and energy consuming.
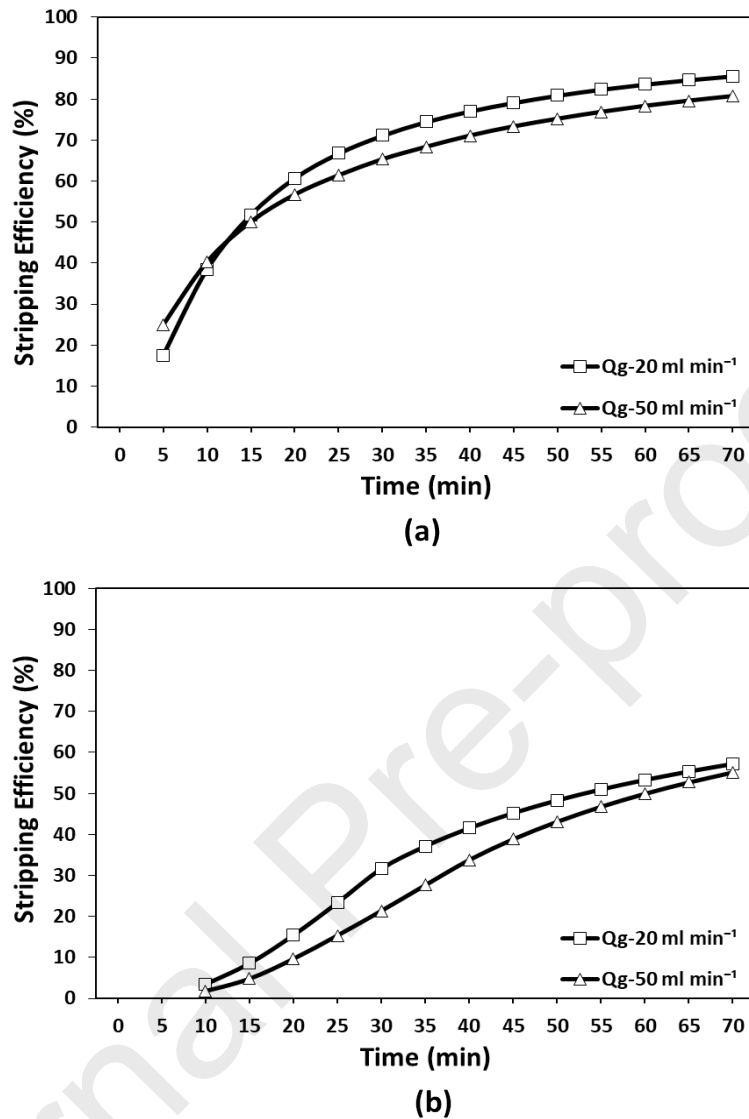

(a)

(b)

Figure 6 Stripping efficiency of the membrane stripper during coupled absorption/desorption against operation time for IL (a) [emim] [MS] and (b) [emim] [DCA]; stripping gas flowrate, $Q_{N_2} = 100\ ml$ min^{-1}

4.2   Pseudo steady state; mass transfer coefficient and enhancement factor

Experimental mass transfer coefficient at pseudo steady state was calculated for two different feed gas flowrates using equation 1 and presented in figure 7. An increase in mass transfer coefficient was observed with increase in feed gas flowrate inside membrane absorber, in most cases except for [emim][MS] during coupled absorption/desorption operation where a minor decrease was observed for increase in feed gas flowrate. The increase in mass transfer coefficient is primarily due to the increase in membrane flux with increase in feed gas flowrate. The exception for [emim][MS] might be due to the lower pseudo steady state efficiency of this IL at higher feed gas flowrates. At higher feed gas flowrate of 50 ml min^{-1}, the IL absorbed more CO$_2$ in membrane absorber due to higher flux and yet retained a high CO$_2$ loading at pseudo steady state, which resulted in the lower mass transfer coefficient. Coupled absorption/desorption process retained a very high mass transfer coefficient of

1.8 10^{-6} m s^{-1} and 2.3 10^{-6} m s^{-1}, for [emim] [MS] and [emim] [DCA], respectively. At the feed gas flowrate of 20 ml min^{-1}, IL [emim] [MS] showed an increase in mass transfer coefficient from 0.2 10^{-6} m s^{-1} to 1.9 10^{-6} m s^{-1}, for single module absorption and coupled absorption/desorption, respectively. For [emim] [DCA], at the same conditions, the increase was from 0.3 10^{-6} m s^{-1} to 1.6 10^{-6} m s^{-1}, for single module absorption and coupled absorption/desorption, respectively. The enhanced mass transfer for coupled absorption/desorption process is due to the lower CO_2 concentration of the ILs. The lower mass transfer coefficients of single module absorption explain the increased mass transfer resistance due to the higher CO_2 concentration of the ILs.
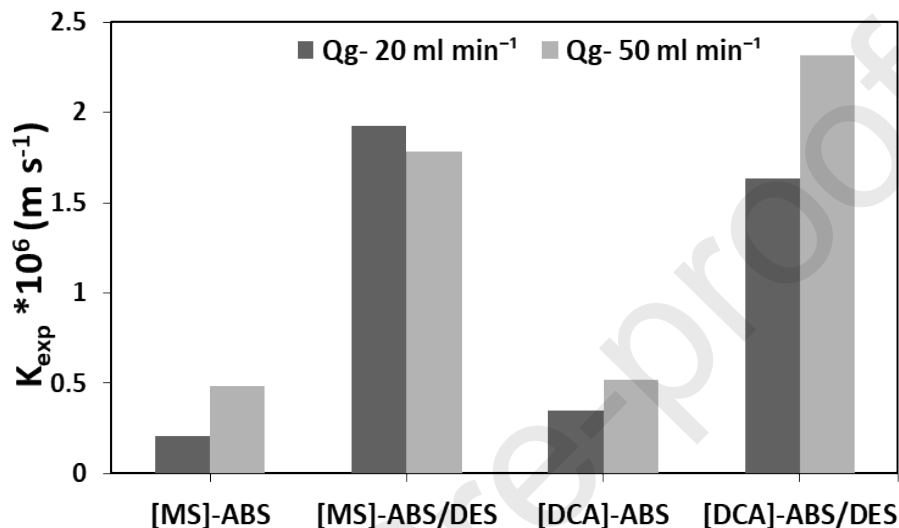

Figure 7 Experimental mass transfer coefficient, K_{exp}, for CO_2 absorption in ILs [emim] [MS] ([MS]) and [emim] [DCA] ([DCA]) during coupled absorption/desorption (ABS/DES) and single module absorption (ABS) at pseudo steady state

The enhancement factor represents the enhancement in mass transfer due to the presence of chemical reaction. Figure 8 presents a comparison of enhancement factor between coupled absorption/desorption and single module absorption, at pseudo steady state. The enhancement factor nearly remained constant after achieving pseudo steady state. An increase in feed gas flowrate has positively affected the enhancement factor except for [emim][MS] during coupled absorption/desorption, where the increase in gas flowrate has decreased the enhancement factor. At feed gas flowrate of 50 ml min^{-1}, enhancement factor of IL [emim][MS] for single module absorption was noted to be of 0.7 magnitude, nearly 4 time less than that of coupled absorption/desorption, which was noted to be 2.6. For IL [emim][DCA], at the same conditions, the single module absorption enhancement factor was noted to be 0.75, nearly 4.5 times less than for coupled absorption/desorption. The above-mentioned high magnitude enhancement factor for coupled absorption/desorption and nearly four-time lower values at single module absorption, verifies the dependency of this factor on the CO_2 concentration in the IL. The coupled process retains the high magnitude of enhancement due to the continuous desorption of CO_2 in the membrane stripper.
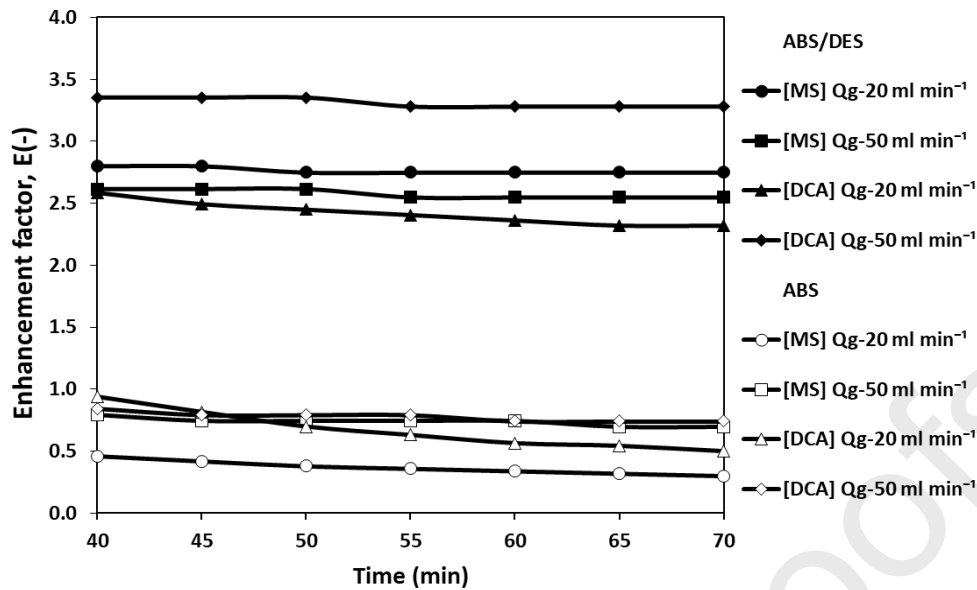
Figure 8 Enhancement factor, E, for CO_2 absorption in ILs [emim] [MS] ([MS]) and [emim] [DCA] ([DCA]) during coupled absorption/desorption (ABS/DES) and single module absorption (ABS) at pseudo steady state

4.3   Model Simulations and discussion

The simulations obtained from the dynamic model developed for the coupled absorption/desorption and single module absorption are presented here. Unloaded IL was considered for countercurrent recirculation on the shell side of membrane absorber and membrane stripper. Gas mixture containing 15 % CO_2 (and N_2 rest to balance), was considered as a feed to the lumen side of membrane absorber in open loop conditions. Pure N_2 passing from the lumen side of membrane stripper was considered as a sweep gas. Simulations of CO_2 removal efficiency were plotted against operation time and presented in figure 9. Efficiency of the coupled absorption/desorption and single module absorption process reduces with time until reaching pseudo steady state. Experimental data (dots in the figure 9) is also presented in the figure to compare it with simulated results. A much-closed agreement was found between simulations and experimental data.
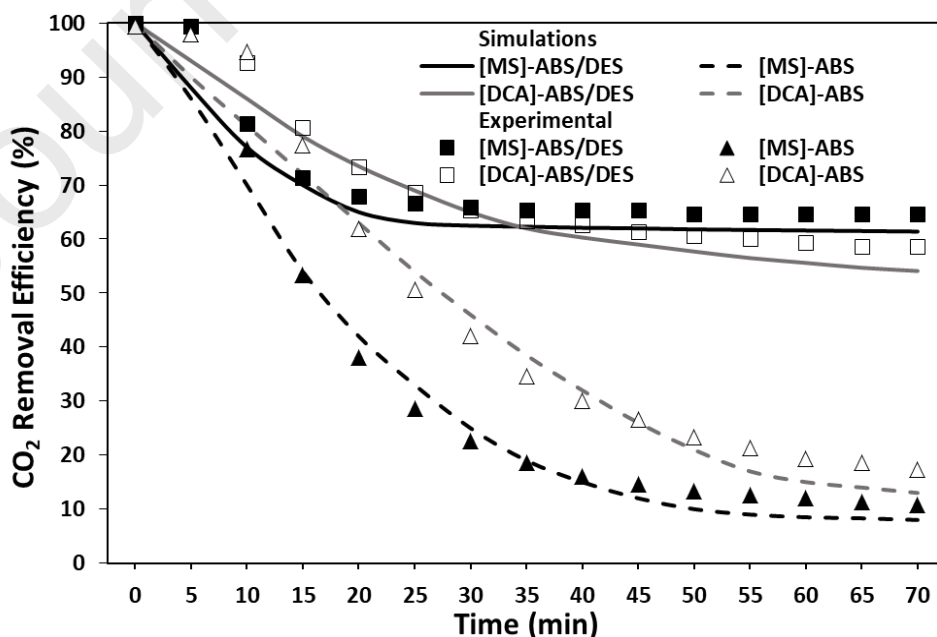
Figure 9 Comparison of simulated and experimental CO_2 removal efficiency of the membrane absorber for coupled absorption/desorption (ABS/DES) and single module absorption (ABS) against operation time; $Q_g = 20 \ ml \ min^{-1}$

A parametric analysis was carried out for coupled absorption/desorption process, to study and compare the effect of porosity of the membrane and sweeping gas flowrate on the gas side outlet CO_2 concentration of the membrane absorber. IL [emim][MS] was selected for current analysis. Obvious effects of sweeping gas flowrate on gas side outlet CO_2 concentration can be observed from figure 10 rather than porosity of membrane. For 60 % porous membrane, increase in sweeping gas flowrate from 50 ml min^{-1} to 200 ml min^{-1}, has decreased the normalized gas side outlet CO_2 concentration from 0.7 to 0.1. It represents an addition of 60 % efficiency to the system. Increase in porosity has not much affected the outlet concentration and efficiency.
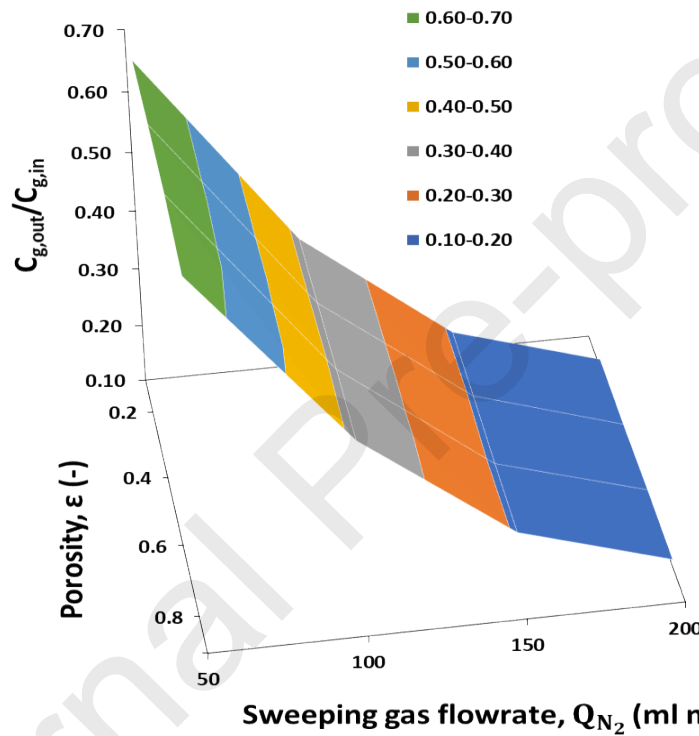

Figure 10 Effect of sweeping gas flowrate and porosity on the outlet concentration of CO_2 in the feed stream for IL [emim][MS]

Another analysis was performed to optimize the sweeping gas flowrate, porosity of the membrane and IL flowrate, to achieve zero CO_2 concentration (100 % efficient stripping) at the membrane stripper outlet, in a single absorption desorption cycle. Simulations have been run with different values for these parameters to achieve zero CO_2 concentration at the membrane stripper outlet. The results of simulation are presented in figure 11. Increase in gas flowrate and membrane porosity and decrease in liquid flowrate were found favorable in achieving the target concentration. For 60 % porous membrane, 48 ml min^{-1} liquid flowrate must be maintained when 200 ml min^{-1} sweeping gas is passed from the membrane stripper. Reducing the sweeping gas flowrate to 50 ml min^{-1}, needs a reduction of 30 ml min^{-1} in the liquid flowrate, to maintain zero CO_2 concentration at the outlet. The gas side outlet concentration of the membrane stripper doesn't look much sensitive to membrane porosity. Sensitivity of the optimization can be ranked as $Q_{IL} > Q_{N_2} > \varepsilon$.
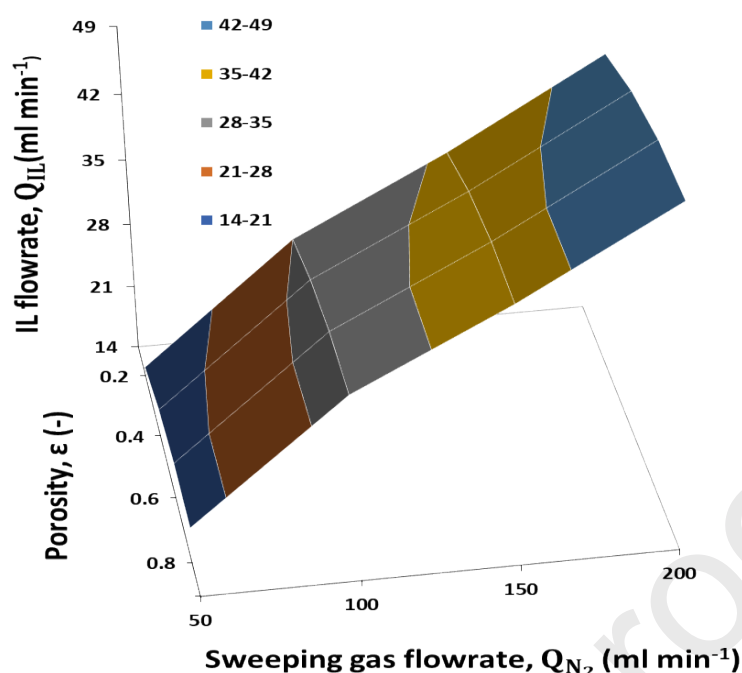
Figure 11 Optimizing sweeping gas flowrate, IL flowrate and membrane porosity for achieving zero concentration of CO_2 at the membrane stripper outlet for IL [emim][MS]

5   Conclusion

The aim of this work was to investigate about two [emim] cation based RTILs that have never been tested for post-combustion CO_2 capture in a membrane contactor. A membrane contactor setup was developed which can work as single module absorption or coupled absorption/desorption. A detailed analysis was carried out to study and compare both setups. Absorption efficiency of the membrane absorber, stripping efficiency of the membrane stripper, CO_2 loading of the IL, mass transfer coefficients and enhancement factors were studied. A dynamic modelling approach was also implemented to perform parametric and optimization studies. The absorption efficiency of the membrane absorber decreased with the operation time until reaching pseudo steady state. For single module absorption, the absorption efficiency could drop to as low as 10 % at pseudo steady state, while the coupled absorption/desorption setup was able to keep the membrane absorber efficiency as high as 90%. Coupled absorption/desorption was able to keep 2-6 folds less maximal loading of CO_2 at pseudo steady state, compared to single module absorption. The mass transfer coefficient and enhancement factors for coupled absorption/desorption were much higher than for single module absorption. Moreover, effects of parameters and optimization of the process to achieve zero CO_2 concentration at the membrane stripper outlet were studied in simulations. The higher pseudo steady state stripping efficiencies of the membrane stripper at ambient conditions confirmed the very physical absorption nature of the two RTILs for CO_2. The desorption might be considered very plain and cost effective. For commercial scale continuous post-combustion carbon capture, the coupled absorption/desorption setup might be very suitable after further modifications and improvements, particularly modifications in the means of desorption inside the membrane stripper.

Appendix A; Shell side mass transfer coefficient

Since IL flows inside the shell of the membrane contactor, the liquid mass transfer coefficient was found by equation 6. The terms, hydraulic diameter d_h and Reynolds number R_e of equation 6 were found from the following equations.

$$R_e = \frac{4\rho_{IL}Q}{\pi\mu_{IL}(d_{c,i} + Nd_0)} \tag{20}$$

$$d_h = \frac{d_{c,i}{}^2 - Nd_o{}^2}{d_{c,i} + Nd_o} \tag{21}$$

Appendix B; Diffusivity of gas inside porous membrane

If the membrane pore diameter is larger than 1 10^{-5} m, bulk diffusion, D_g (equation 14) is dominant; if it is less than 1 10^{-7} m, Knudsen diffusion is dominant. In case of pore diameter between above two values, both types of diffusion can exist.

$$\frac{1}{D_m} = \frac{1}{D_g} + \frac{1}{D_{Kn}} \tag{22}$$

D_{Kn} in the above equation is known as Knudsen diffusion coefficient, which can be found as below.

$$D_{Kn} = \frac{1}{2}d_p\sqrt{\frac{8RT}{\pi M}} \tag{23}$$

If the membrane is considered completely gas filled and the only mass transfer resistance inside the membrane is considered to be the membrane itself, effective diffusion coefficient can be applied.

$$D_m = D_{eff} = \frac{\varepsilon D_g}{\tau} \tag{24}$$

References

Albo, J., Irabien, A., 2012. Non-dispersive absorption of CO 2 in parallel and cross-flow membrane modules using EMISE. J. Chem. Technol. Biotechnol. 87, 1502–1507. https://doi.org/10.1002/jctb.3790

Albo, J., Luis, P., Irabien, A., 2010. Carbon Dioxide Capture from Flue Gases Using a Cross-Flow Membrane Contactor and the Ionic Liquid 1-Ethyl-3-methylimidazolium Ethylsulfate. Ind. Eng. Chem. Res. 49, 11045–11051. https://doi.org/10.1021/ie1014266

Anthony, J.L., Maginn, E.J., Brennecke, J.F., 2002. Solubilities and thermodynamic properties of gases in the ionic liquid 1-n-butyl-3-methylimidazolium hexafluorophosphate. J. Phys. Chem. B. https://doi.org/10.1021/jp020631a

Barbe, A.M., Hogan, P.A., Johnson, R.A., 2000. Surface morphology changes during initial usage of hydrophobic, microporous polypropylene membranes. J. Memb. Sci. https://doi.org/10.1016/S0376-7388(00)00338-0

Blanchard, L.A., Hancu, D., Beckman, E.J., Brennecke, J.F., 1999. Green processing using ionic liquids and CO2. Nature. https://doi.org/10.1038/19887

Brennecke, J.F., Gurkan, B.E., 2010. Ionic liquids for CO2 capture and emission reduction. J. Phys. Chem. Lett. https://doi.org/10.1021/jz1014828

Chen, Y., Mutelet, F., Jaubert, J.N., 2012. Modeling the solubility of carbon dioxide in imidazolium-based ionic liquids with the PC-SAFT equation of state. J. Phys. Chem. B. https://doi.org/10.1021/jp309944t

Costa, A.J.L., Esperanca, M.S.S., Marrucho, I.M., Rebelo, L.P.N., 2011. Densities and Viscosities of 1-Ethyl-3-methylimidazolium n -Alkyl Sulfates. J. Chem. Eng. Data 56, 3433–3441.

Cui, Z., Demontigny, D., 2013. Part 7: A review of CO2 capture using hollow fiber membrane contactors. Carbon Manag. https://doi.org/10.4155/cmt.12.73

Demontigny, D., Tontiwachwuthikul, P., Chakma, A., 2005. Comparing the absorption performance of packed columns and membrane contactors. Ind. Eng. Chem. Res. https://doi.org/10.1021/ie040264k

Drioli, E., Stankiewicz, A.I., Macedonio, F., 2011. Membrane engineering in process intensification-An overview. J. Memb. Sci. https://doi.org/10.1016/j.memsci.2011.06.043

Falk-Pedersen, O., Grønvold, M.S., Nøkleby, P., Bjerve, F., Svendsen, H.F., 2005. CO 2 Capture with Membrane Contactors . Int. J. Green Energy. https://doi.org/10.1081/ge-200058965

Figueroa, J.D., Fout, T., Plasynski, S., McIlvried, H., Srivastava, R.D., 2008. Advances in CO2 capture technology-The U.S. Department of Energy's Carbon Sequestration Program. Int. J. Greenh. Gas Control. https://doi.org/10.1016/S1750-5836(07)00094-1

Franken, A.C.M., Nolten, J.A.M., Mulder, M.H.V., Bargeman, D., Smolders, C.A., 1987. Wetting criteria for the applicability of membrane distillation. J. Memb. Sci. https://doi.org/10.1016/S0376-7388(00)80288-4

Fuller, E.N., Schettler, P.D., Giddings, J.C., 1966. A new method for prediction of binary gas-phase diffusion coefficients. Ind. Eng. Chem. 58, 18–27. https://doi.org/10.1021/ie50677a007

Gabelman, A., Hwang, S.-T., 1999. Hollow fiber membrane contactors. J. Memb. Sci. 159, 61–106. https://doi.org/10.1016/S0376-7388(99)00040-X

Gómez-Coma, L., Garea, A., Irabien, A., 2014. Non-dispersive absorption of CO2 in [emim][EtSO4] and [emim][Ac]: Temperature influence. Sep. Purif. Technol. 132, 120–125. https://doi.org/10.1016/j.seppur.2014.05.012

Gómez-Coma, L., Garea, A., Irabien, Á., 2017. Hybrid Solvent ([emim][Ac]+water) to Improve the CO2Capture Efficiency in a PVDF Hollow Fiber Contactor. ACS Sustain. Chem. Eng. 5, 734–743. https://doi.org/10.1021/acssuschemeng.6b02074

Happel, J., 1959. Viscous flow relative to arrays of cylinders. AIChE J. 5, 174–177. https://doi.org/10.1002/aic.690050211

Huang, K., Peng, H.L., 2017. Solubilities of Carbon Dioxide in 1-Ethyl-3-methylimidazolium Thiocyanate, 1-Ethyl-3-methylimidazolium Dicyanamide, and 1-Ethyl-3-methylimidazolium Tricyanomethanide at (298.2 to 373.2) K and (0 to 300.0) kPa. J. Chem. Eng. Data. https://doi.org/10.1021/acs.jced.7b00476

IPCC, 2005. IPCC special report on carbon dioxide capture and storage. Prepared by working group III of the Intergovernmental Panel on Climate Change, in: IPCC Special Report on Carbon Dioxide Capture and Storage. https://doi.org/10.1002/anie.201000431

Kladkaew, N., Idem, R., Tontiwachwuthikul, P., Saiwan, C., 2011. Studies on corrosion and corrosion inhibitors for amine based solvents for CO2 absorption from power plant flue gases containing CO2, O2 and SO2, in: Energy Procedia. https://doi.org/10.1016/j.egypro.2011.02.051

Klomfar, J., Součková, M., Pátek, J., 2011. Temperature dependence of the surface tension and density at 0.1 MPa for 1-ethyl- and 1-butyl-3-methylimidazolium dicyanamide. J. Chem. Eng. Data. https://doi.org/10.1021/je200502j

Kothandaraman, A., 2010. Carbon Dioxide Capture by Chemical Absorption : A Solvent Comparison Study. Carbon N. Y.

Li, J.L., Chen, B.H., 2005. Review of CO2 absorption using chemical solvents in hollow fiber membrane contactors. Sep. Purif. Technol. https://doi.org/10.1016/j.seppur.2004.09.008

Lu, J.G., Hua, A.C., Xu, Z.W., Li, J.T., Liu, S.Y., Wang, Z.L., Zhao, Y.L., Pan, C., 2013. CO2capture by membrane absorption coupling process: Experiments and coupling process evaluation. J. Memb. Sci. 431, 9–18. https://doi.org/10.1016/j.memsci.2012.12.039

Lu, J.G., Lu, C.T., Chen, Y., Gao, L., Zhao, X., Zhang, H., Xu, Z.W., 2014. CO2capture by membrane absorption coupling process: Application of ionic liquids. Appl. Energy 115, 573–581. https://doi.org/10.1016/j.apenergy.2013.10.045

Lu, J.G., Lu, Z.Y., Chen, Y., Wang, J.T., Gao, L., Gao, X., Tang, Y.Q., Liu, D.G., 2015. CO$_2$ absorption into aqueous blends of ionic liquid and amine in a membrane contactor. Sep. Purif. Technol. 150, 278–285. https://doi.org/10.1016/j.seppur.2015.07.010

Luis, P., Garea, A., Irabien, A., 2009. Zero solvent emission process for sulfur dioxide recovery using a

membrane contactor and ionic liquids. J. Memb. Sci. 330, 80–89. https://doi.org/10.1016/j.memsci.2008.12.046

Makhloufi, C., Lasseuguette, E., Remigy, J.C., Belaissaoui, B., Roizard, D., Favre, E., 2014. Ammonia based CO2 capture process using hollow fiber membrane contactors. J. Memb. Sci. https://doi.org/10.1016/j.memsci.2013.12.063

Mansourizadeh, A., Ismail, A.F., 2009. Hollow fiber gas-liquid membrane contactors for acid gas capture: A review. J. Hazard. Mater. https://doi.org/10.1016/j.jhazmat.2009.06.026

Mejía, I., Stanley, K., Canales, R., Brennecke, J.F., 2013. On the high-pressure solubilities of carbon dioxide in several ionic liquids. J. Chem. Eng. Data 58, 2642–2653. https://doi.org/10.1021/je400542b

Morgan, D., Ferguson, L., Scovazzo, P., 2005. Diffusivities of gases in room-temperature ionic Liquids: Data and correlations obtained using a lag-time technique. Ind. Eng. Chem. Res. 44, 4815–4823. https://doi.org/10.1021/ie048825v

Mosadegh-Sedghi, S., Rodrigue, D., Brisson, J., Iliuta, M.C., 2014. Wetting phenomenon in membrane contactors - Causes and prevention. J. Memb. Sci. https://doi.org/10.1016/j.memsci.2013.09.055

Ortiz, A., Gorri, D., Irabien, Á., Ortiz, I., 2010. Separation of propylene/propane mixtures using Ag+-RTIL solutions. Evaluation and comparison of the performance of gas-liquid contactors. J. Memb. Sci. 360, 130–141. https://doi.org/10.1016/j.memsci.2010.05.013

Qazi, S., Gómez-coma, L., Albo, J., Druon-bocquet, S., Irabien, A., 2019. Mathematical Modelling of CO 2 Absorption with Ionic Liquids in a Membrane Contactor , Study of Absorption Kinetics and Influence of Temperature. J Chem Technol Biotechnol. https://doi.org/10.1002/jctb.6265

Qazi, S., Gómez-Coma, L., Albo, J., Druon-Bocquet, S., Irabien, A., Sanchez-Marcano, J., 2020. CO2 capture in a hollow fiber membrane contactor coupled with ionic liquid: Influence of membrane wetting and process parameters. Sep. Purif. Technol. https://doi.org/10.1016/j.seppur.2019.115986

Qi, Z., Cussler, E.L., 1985. Microporous hollow fibers for gas absorption. J. Memb. Sci. https://doi.org/10.1016/s0376-7388(00)83150-6

Quijada-Maldonado, E., Van Der Boogaart, S., Lijbers, J.H., Meindersma, G.W., De Haan, A.B., 2012. Experimental densities, dynamic viscosities and surface tensions of the ionic liquids series 1-ethyl-3-methylimidazolium acetate and dicyanamide and their binary and ternary mixtures with water and ethanol at T = (298.15 to 343.15 K). J. Chem. Thermodyn. 51, 51–58. https://doi.org/10.1016/j.jct.2012.02.027

Rahman, F.A., Aziz, M.M.A., Saidur, R., Bakar, W.A.W.A., Hainin, M.R., Putrajaya, R., Hassan, N.A., 2017. Pollution to solution: Capture and sequestration of carbon dioxide (CO 2) and its utilization as a renewable energy source for a sustainable future. Renew. Sustain. Energy Rev. https://doi.org/10.1016/j.rser.2017.01.011

Ramdin, M., De Loos, T.W., Vlugt, T.J.H., 2012. State-of-the-art of CO \n 2 capture with ionic liquids. Ind. Eng. Chem. Res. 51, 8149–8177. https://doi.org/10.1021/ie3003705

Rangwala, H.A., 1996. Absorption of carbon dioxide into aqueous solutions using hollow fiber membrane contactors. J. Memb. Sci. https://doi.org/10.1016/0376-7388(95)00293-6

Rogers, R.D., Seddon, K.R., 2003. Ionic Liquids - Solvents of the Future? Science (80-.). https://doi.org/10.1126/science.1090313

Sander, R., 2015. Compilation of Henry's law constants (version 4.0) for water as solvent. Atmos. Chem. Phys. 15, 4399–4981. https://doi.org/10.5194/acp-15-4399-2015

Santos, C.S., Baldelli, S., 2009. Alkyl Chain Interaction at the Surface of Room Temperature Ionic Liquids: Systematic Variation of Alkyl Chain Length (R = C 1 –C 4 , C 8) in both Cation and Anion of [RMIM][R – OSO 3] by Sum Frequency G. J. Phys. Chem. B 113, 923–933. https://doi.org/10.1021/jp807924g

Shen, S., Kentish, S.E., Stevens, G.W., 2010. Shell-side mass-transfer performance in hollow-fiber membrane contactors. Solvent Extr. Ion Exch. https://doi.org/10.1080/07366299.2010.515176

Shiflett, M.B., Drew, D.W., Cantini, R.A., Yokozeki, A., 2010. Carbon dioxide capture using ionic liquid 1-butyl-3-methylimidazolium acetate. Energy and Fuels. https://doi.org/10.1021/ef100868a

Sumon, K.Z., Henni, A., 2011. Ionic liquids for CO2 capture using COSMO-RS: Effect of structure, properties and molecular interactions on solubility and selectivity. Fluid Phase Equilib. https://doi.org/10.1016/j.fluid.2011.06.038

Vaidya, P.D., Kenig, E.Y., 2007. CO2-alkanolamine reaction kinetics: A review of recent studies. Chem. Eng. Technol. https://doi.org/10.1002/ceat.200700268

Wang, R., Li, D.F., Zhou, C., Liu, M., Liang, D.T., 2004. Impact of DEA solutions with and without CO 2 loading on porous polypropylene membranes intended for use as contactors. J. Memb. Sci. https://doi.org/10.1016/j.memsci.2003.10.022

Wang, X., Chen, H., Zhang, L., Yu, R., Qu, R., Yang, L., 2014. Effects of coexistent gaseous components and fine particles in the flue gas on CO2 separation by flat-sheet polysulfone membranes. J. Memb. Sci. https://doi.org/10.1016/j.memsci.2014.07.040

Yim, J.H., Ha, S.J., Lim, J.S., 2018. Measurement and Correlation of CO2Solubility in 1-Ethyl-3-methylimidazolium ([EMIM]) Cation-Based Ionic Liquids: [EMIM][Ac], [EMIM][Cl], and [EMIM][MeSO4]. J. Chem. Eng. Data 63, 508–518. https://doi.org/10.1021/acs.jced.7b00532

Yu, C.H., Huang, C.H., Tan, C.S., 2012. A review of CO2 capture by absorption and adsorption. Aerosol Air Qual. Res. https://doi.org/10.4209/aaqr.2012.05.0132

Yu, K.M.K., Curcic, I., Gabriel, J., Tsang, S.C.E., 2008. Recent advances in CO2 capture and utilization. ChemSusChem. https://doi.org/10.1002/cssc.200800169

Zhang, H.Y., Wang, R., Liang, D.T., Tay, J.H., 2008. Theoretical and experimental studies of membrane wetting in the membrane gas-liquid contacting process for CO2 absorption. J. Memb. Sci. https://doi.org/10.1016/j.memsci.2007.09.050

Zhang, L., Qu, R., Sha, Y., Wang, X., Yang, L., 2015. Membrane gas absorption for CO2 capture from flue gas containing fine particles and gaseous contaminants. Int. J. Greenh. Gas Control. https://doi.org/10.1016/j.ijggc.2014.11.017

Zhao, S., Feron, P.H.M., Cao, C., Wardhaugh, L., Yan, S., Gray, S., 2015. Membrane evaporation of amine solution for energy saving in post-combustion carbon capture: Wetting and condensation. Sep. Purif. Technol. https://doi.org/10.1016/j.seppur.2015.03.015

Zhao, S., Feron, P.H.M., Deng, L., Favre, E., Chabanon, E., Yan, S., Hou, J., Chen, V., Qi, H., 2016. Status and progress of membrane contactors in post-combustion carbon capture: A state-of-the-art review of new developments. J. Memb. Sci. 511, 180–206. https://doi.org/10.1016/j.memsci.2016.03.051
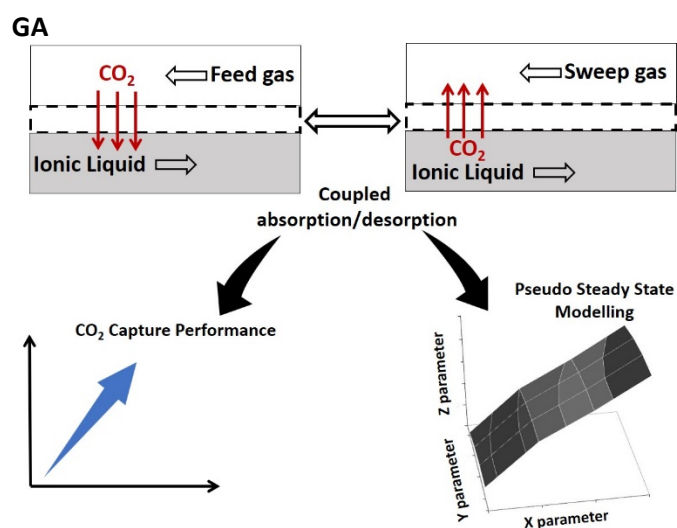
Highlights:

- Coupled Absorption/Desorption and Single Module Absorption setups were developed for CO_2 capture
- Imidazolium based room temperature ionic liquids were coupled with membrane absorber and stripper
- A pseudo-steady state modeling approach was also implemented for sensitivity and parametric analysis
- Coupled Absorption/Desorption arrangement was able to keep long term high absorption performance
- Long term zero CO_2 concentration at stripper outlet was simulated by optimizing the operating parameters

Declaration of interests

☒ The authors declare that they have no known competing financial interests or personal relationships that could have appeared to influence the work reported in this paper.

☐The authors declare the following financial interests/personal relationships which may be considered as potential competing interests:

Credit Author Statement

S. No.	First Name, Sur Name	Role
1.	Qazi Sohaib	Investigation, Conceptualization, Validation, Formal analysis, Data Curation, Software, Writing - Original Draft
2.	Jose Manuel Vadillo	Investigation
3.	Lucía Gómez-Coma	Supervision, Methodology, Writing - Review & Editing
4.	Jonathan Albo	Supervision, Methodology, Writing - Review & Editing
5.	Stéphanie Druon-Bocquet	Supervision, Writing - Review & Editing
6.	Angel Irabien	Supervision, Project administration, Writing - Review & Editing
7.	José Sanchez-Marcano	Supervision, Conceptualization, Project administration, Writing - Review & Editing